NACA RM L58C24

NACA

RESEARCH MEMORANDUM

TESTS OF AERODYNAMICALLY HEATED MULTIWEB WING STRUCTURES IN A FREE JET AT MACH NUMBER 2

AN ALUMINUM-ALLOY MODEL OF 40-INCH CHORD WITH 0.125-INCH-THICK SKIN

By George E. Griffith and Georgene H. Miltonberger

Langley Aeronautical Laboratory
Langley Field, Va.

NATIONAL ADVISORY COMMITTEE FOR AERONAUTICS

WASHINGTON

June 23, 1958
Declassified February 8, 1960

NACA RM L58C24

NATIONAL ADVISORY COMMITTEE FOR AERONAUTICS

RESEARCH MEMORANDUM

TESTS OF AERODYNAMICALLY HEATED MULTIWEB WING STRUCTURES IN A FREE JET AT MACH NUMBER 2

AN ALUMINUM-ALLOY MODEL OF 40-INCH CHORD WITH 0.125-INCH-THICK SKIN

By George E. Griffith and Georgene H. Miltonberger

SUMMARY

A 5-percent-thick 2024-T3 aluminum-alloy multiweb wing (MW-1-(2)), a duplicate of multiweb wing MW-1 which was the first in a series of wings previously reported upon, was also tested at a Mach number of 2 under simulated supersonic flight conditions. The duplicate model experienced a dynamic failure as a result of a catastrophic flag-waving type of flutter due to the combined action of aerodynamic heating and loading. The failure is discussed and compared with the failure of the original wing; the temperature data for the two models are also compared. For model MW-1-(2), generally fair agreement was obtained between experimental and calculated temperatures, pressures, and strains.

INTRODUCTION

The first in a series of representative airplane or missile wings tested at a Mach number of 2 under simulated sea-level flight conditions experienced an unexpected and violent dynamic failure. This wing structure (MW-1) was made of 2024-T3 aluminum alloy, had a 5-percent-thick circular-arc airfoil, contained six equally spaced spanwise webs, was of 40-inch chord and semispan, and was instrumented with 22 thermocouples; the results of the test and the model failure were reported in reference 1. After this test, several additional models were constructed and equipped with varying degrees of instrumentation (thermocouples, pressure devices, and strain gages); when these structures were similarly tested, some additional failures resulted. These latter models also had 5-percent-thick circular-arc airfoils, and were made of various materials (steel, magnesium, and aluminum alloy), but were of 20-inch chord and

semispan and incorporated various structural changes in the skin, tip bulkhead, and internal design. References 2 and 3 discuss the results of the tests of some of these structures.

In a few cases, duplicates of a given structure were tested in an attempt to provide, through increased instrumentation and higher speed photography, additional information about a model failure or to determine if a similar type of failure would recur (ref. 4). The present paper discusses the test results of multiweb wing MW-1-(2) and compares the test results with those for the original multiweb wing MW-1. Whereas the original wing was instrumented only with thermocouples, model MW-1-(2) was equipped to give pressure and strain data as well as temperatures; in addition, motion pictures of the behavior of the duplicate model (MW-1-(2)) were obtained at up to 1,600 frames per second compared with 24 frames per second for the original structure.

SYMBOLS

C_p	pressure coefficient, $\left(p - p_\infty\right)\Big/q_\infty$
h	aerodynamic heat-transfer coefficient, Btu/(sq ft)(sec)($^\circ$F)
p	static pressure, psia
p_t	stagnation pressure, psia
p_∞	free-stream static pressure, psia
q_∞	free-stream dynamic pressure, psi
T	temperature, $^\circ$F
T_{aw}	adiabatic wall temperature, $^\circ$F
T_o	initial temperature, $^\circ$F
T_t	stagnation temperature, $^\circ$F
T_∞	free-stream temperature, $^\circ$F
t	time, sec

TEST PROCEDURE

Model

Within fabrication tolerances, model MW-1-(2) was a duplicate of model MW-1 (ref. 1) which was an idealized 40-inch-semispan cantilever multiweb wing with a 5-percent-thick, symmetrical, circular-arc airfoil section of 40-inch chord. The model had 0.125-inch-thick skin, six equally spaced 0.072-inch-thick internal longitudinal webs, and solid leading- and trailing-edge sections, all of 2024-T3 aluminum alloy. A solid 1-inch-thick steel bulkhead was located at the tip of the model, and at the root a solid steel bulkhead extended $2\frac{1}{2}$ inches into the model and also attached the model to its mounting support. External doubler plates of 1/8-inch-thick 2024-T3 aluminum alloy were added to strengthen the model at the root. Pertinent dimensions and details of construction are given in figure 1.

Measurements made after the model was assembled indicated that the maximum permanent or built-in twist, with respect to the tip of the model, of any chordwise section was less than 0.08°.

Before testing, the exterior of the wing was painted with a thin layer of zinc chromate and then striped with black lacquer to form a grid pattern (see fig. 2) to aid in studying the model behavior recorded by the high-speed motion pictures.

Natural Modes and Frequencies

The first twelve natural modes and frequencies for model MW-1-(2) were obtained at room temperature prior to the aerodynamic test. The data are recorded in figure 3; no similar data are available for the original model (MW-1). All but the first three simple mode shapes presented in figure 3 show appreciable chordwise distortion, which indicates that the chordwise stiffness of this model is low.

Model Instrumentation

The model was instrumented with thermocouples, wire strain gages, pressure orifices, and an accelerometer. (See fig. 4.) Thirty-five iron-constantan thermocouples were installed: 21 were peened into the skin, 8 were peened into the internal webs, and 6 were inserted in holes in the solid leading and trailing edges (as shown in fig. 4). However,

because of data recording limitations, only 28 thermocouples were used in the test, and during the test one thermocouple (32) did not function properly.

Fourteen pressure orifices were located across the chord on one surface of the model so as to correspond approximately with the center line of the jet; pressures were obtained at 10 stations and differential pressures were obtained between the two opposite surfaces $1\frac{7}{8}$ inches inboard of both the solid leading and trailing edges. The orifices were connected by tubing to six-capsule manometers.

Thirteen SR-4 type EBDF-7D temperature-compensated wire strain gages were attached to the model and cured in two cycles to temperatures of 270° F and 285° F. Calibration data for the individual gages were obtained only during these two cycles. Twelve of the gages were attached to the underside of the skin, ten in the chordwise direction - primarily to obtain information about the frequency and phasing of any vibration or flutter of the individual skin panels - and two in the spanwise direction. The two spanwise skin gages were used in an attempt to obtain the magnitudes of any induced strains at these two points; one other gage was attached to the third web inboard of the leading edge at the center line of the web and in the longitudinal direction to pick up any spanwise strain in the stiffener.

A 10g accelerometer which weighed less than 6 grams was attached to the underside of the skin in the next to last bay for the purpose of measuring any vibratory or flutter frequencies of the model in a direction perpendicular to the skin surface.

Supplementary data were supplied through 16-millimeter motion-picture cameras operating at approximately 128, 600, 1,000, and 1,600 frames per second; these cameras were located overhead and opposite the sides of the model.

Accuracy

The estimated probable errors in the individual measurements for both the tunnel data and the data from the model instrumentation are presented in the following table along with the corresponding time constants:

Item	Probable error	Time constant
Tunnel stagnation pressure	±0.7 psi	0.03 sec
[a]Tunnel stagnation temperature . .	±3° F	.12 sec
Model temperature	±3° F	.03 sec
Model pressure	±0.1 psi	.03 sec
Model strain	±80 μin./in.	.02 sec

[a]The probable error for the tunnel stagnation temperature does not include any error in the reference or cold-junction temperature (to be discussed later).

Errors due to the thermocouple installation are not included but should have been very small, except when the skin thermocouples were undergoing appreciable vibrations - at which time the contact between the thermocouples and skin may have varied - and except possibly for the leading and trailing edges where installation was somewhat more difficult than for the peened-in thermocouples. The reported skin temperatures, measured near the inside surface of the skin, should be within 2° F of the average skin temperature except when the skin was subjected to appreciable vibration. The Mach number was 2.00 ± 0.02.

In order to ensure accurate determination of the timing of events depicted in the motion pictures, the same accurate timing supplied to the oscillograph records was made visible in the field of view of the motion-picture cameras.

Description of Test

The wing was tested in a free jet at the exit of a Mach number 2, 27- by 27-inch nozzle in the preflight jet, a blowdown wind tunnel located at the Langley Pilotless Aircraft Research Station at Wallops Island, Va. (For additional details concerning this facility, see ref. 2.) The model was mounted vertically, root downward (fig. 2), along the center line of the jet such that the chord plane at the tip of the model was perpendicular to the nozzle exit in order to position the model at an angle of attack of 0°. The leading edge of the wing was located 1 inch downstream of the nozzle exit plane. The top 4 inches of the wing and the 9 inches above the root extended above and below the airstream. Although guy cables were used to stabilize the wing tip for the MW-1 wing (ref. 1), they were not used in the present test.

The model survived the starting disturbance of the jet without difficulty and then remained steady until 5.81 seconds. From this time until 6.29 seconds the model experienced a flag-waving or chordwise

bending type of flutter of very small amplitude. The wing then steadied until 8.14 seconds at which time the wing experienced a similar type of flutter, but as the test progressed the amplitudes gradually increased until at 11.16 seconds (at about the end of test conditions) the model began to break up and thereafter experienced a partial dynamic failure during the shutdown phase of the jet.

Test Conditions

During the test the average aerodynamic conditions, as determined from tunnel data, were: Mach number, 2.00; stagnation pressure, 113 psia; and stagnation temperature, 574° F. (As will be seen later, some doubt exists concerning this value of the stagnation temperature.) These and other pertinent aerodynamic data are given in table I.

Tunnel stagnation pressure.- A plot of the variation with time of the stagnation pressure is given in figure 5(a). The curve shown represents an average of two pressures which differed by less than 2.5 psi and which were obtained from total-pressure tubes located just downstream of the heat accumulator. The period of test conditions was determined from this plot and was considered to be the time during which the stagnation pressure equaled or exceeded 100 psia, that is, from 1.6 to 11.3 seconds. Except for an initial peak, the pressure is nearly constant during this period but can be seen to have dropped slightly during the latter portion of the test. The average or mean value of 113 psia was obtained from an integration of the area under the curve during the period of test conditions.

Tunnel stagnation temperature.- A plot of the tunnel stagnation temperature, obtained by averaging the temperatures from five thermocouples located in the screen section of the tunnel (just downstream of the heat accumulator), is shown in figure 5(b). All five thermocouples agreed within 30° F, in contrast to the 115° F spread recorded by the nine thermocouples used in determining the stagnation temperature for model MW-1. (See ref. 1.) However, because of some doubt about the exact cold-junction temperature at the time of the test (the cold-junction temperature may have been as much as 70° F lower than the supposed value), the average value of 574° F derived from the curve of figure 5(b) for the period of test conditions may not reliably represent the true condition existing in the stream near the model. Hence, in comparing the test results of model MW-1-(2) with the test results of the original model, the stagnation temperature used was derived from the temperature data for the model as discussed subsequently in the section entitled "Skin Temperatures."

RESULTS AND DISCUSSION

A motion-picture film supplement has been prepared and is available on loan. A request card form and a description of the film will be found at the back of this paper, on the page immediately preceding the abstract and index page.

Model Temperatures

One of the purposes of this paper is to compare the test results and behavior of model MW-1-(2) with the test results and behavior of the original model, MW-1. Aside from the motion pictures, the temperature data present the only source of information common to both models and also provide an indirect manner of comparing thermal stresses; hence, the temperature data for the two wings will be discussed in some detail. In order to facilitate comparison, some of the temperature data will be presented in dimensionless form.

Recorded model temperatures for all thermocouples in working order are listed in table II at 1-second intervals for as long as temperature data were obtained, but data beyond 11 seconds are of questionable value since test conditions no longer prevail.

Skin temperatures.- The data show, as expected, that the skin temperatures at any given time are highest near the leading edge and drop off exponentially across the chord. There were insufficient data to indicate a spanwise trend. Four of the skin thermocouples (9, 13, 21, and 22) appear to show an unexpected decrease in the rate of change of temperature with respect to time, followed by an increased rate rather than the gradual decrease in rate predicted by theory. This phenomenon is initiated at about 6 seconds, or shortly after the model first began to flutter, and may be the result of temporary loss of intimate contact, or of intermittent contact of the peened-in thermocouple beads with the surrounding metal, initiated by the skin fluctuations during flutter. (All of these thermocouples subsequently became inoperative shortly after the second (and more severe) flutter began.)

Plotted in figure 6 are typical skin temperature histories for model MW-1-(2) and for model MW-1 at approximately the corresponding chordwise location. Figure 6 shows that model MW-1 experienced a greater temperature increase with respect to time and therefore more aerodynamic heating than did model MW-1-(2); this fact is evidenced by the difference between the two curves shown by the shaded area after the curves were made to originate at the same point. Since the aerodynamic heat-transfer coefficients for the two tests should have been essentially the same, a

higher heating rate would be expected for the original model, provided the stagnation temperatures were the same (or nearly so), since its initial temperature was lower; for these conditions the temperature curves would converge near the equilibrium temperature (T_{aw}). However, since the curves actually cross after only a brief heating period, the lower heating rate of model MW-1-(2) must also reflect a lower actual stagnation temperature for this wing than for the original wing. Some doubt about the tunnel stagnation temperature for the test of model MW-1-(2) has already been expressed in the section entitled "Tunnel Stagnation Temperature." Although the exterior of model MW-1-(2) was covered by a thin layer of zinc-chromate paint, whereas the surface of model MW-1 was not, the paint is not considered to have affected the heating rate seriously since the insulating effect of so thin a layer of this paint is almost negligible. (See, for example, ref. 5.)

The combination of relatively thick skin (0.125 inch) and short test run (approximately 10 seconds) prevented the skin from approaching steady-state temperatures, as was also the case for model MW-1. Consequently, the method described in reference 1 was again used to obtain "indicated" values of the adiabatic wall temperatures and the aerodynamic heat-transfer coefficients from the skin temperatures for thermocouples located midway between stiffeners. These values are shown in figure 7 along with similar data previously obtained for model MW-1. In addition, the indicated aerodynamic heat-transfer coefficients are compared with theoretical values calculated according to the theories of Colburn (as given in ref. 6) and Van Driest (ref. 7). Since considerable research in the past few years has shown that the theory of Van Driest is generally more applicable than that of Colburn, comparison of calculated values and additional test data will be restricted to calculations obtained by the Van Driest method; the Colburn curve shown in figure 7 was included because it appeared in the original presentation of the model MW-1 data (ref. 1). Van Driest's method for obtaining values of h involves a knowledge of the ratio of the skin temperature to the free-stream temperature; in figure 7 two curves are plotted, one wherein the skin temperature was assumed equal to the free-stream temperature, and the other in which the skin temperature was assumed equal to the adiabatic wall temperature. Inasmuch as the test data are actually representative of a condition somewhere between these two conditions and since the variation in h is small, an average value of h (at any station) will henceforth be used. Indicated values of h (fig. 7) show a rather large scatter but the values for the two models are in fair agreement, which should be expected since all conditions affecting h were essentially the same. For the forward half of the models, the indicated values of h are in better agreement with values calculated according to Colburn's method, whereas for the latter half of the model the agreement with values predicted by Van Driest's method is better; however, because

of the scatter in the indicated points, the agreement with either theory, though only fair, is about as good as could be expected.

The indicated values of T_{aw} for model MW-1-(2) are generally lower than those for model MW-1; numerical averages give 418° F for model MW-1-(2) and 446° F for the original wing (theoretically there is little change in T_{aw} across the chord). Of importance, as far as aerodynamic heating is concerned, is that $T_{aw} - T_o$ for model MW-1-(2) - using the indicated value of T_{aw} and an average value of T_o - is 338° F compared with 396° F for model MW-1. This would produce faster surface heating in the original wing since the value of $T_{aw} - T_o$ is approximately 20 percent higher than for model MW-1-(2).

When the typical skin temperatures shown in figure 6 are reduced to nondimensional form and compared with values calculated by using Van Driest's heat-transfer coefficients, the results are as shown in figure 8. Actual rather than nondimensional time is used for the plots since all quantities (including h) contained in the appropriate dimensionless time parameter were considered to be essentially the same for the two wings. The dimensionless temperature data for the two wings appear to be in fairly good agreement but are somewhat higher than the calculated temperature ratios. Since generally good overall agreement between the test data for the two wings was obtained, it would appear that the average values of the indicated adiabatic wall temperatures were fairly indicative of the true test conditions and therefore that use of the indicated adiabatic wall temperatures in evaluating the test data is reasonable.

Temperature differences between skin and web center line.- Since no experimental stress distributions are available for the models, a very approximate indication of the relative magnitudes of the induced thermal stresses can be obtained from a comparison of the differences between appropriate skin and web center-line temperatures. However, thermocouples 12 and 17 provided the only temperatures measured at the midheight of the webs for model MW-1-(2), and thus only two experimental temperature differences are available. The difference in temperature between thermocouple 9 in the skin in the second bay (from the leading edge) and thermocouple 12 in the second web, the difference in temperature between thermocouple 13 in the skin in the third bay and thermocouple 17 in the third web, and the results for corresponding locations for model MW-1 have been plotted in figure 9(a). The temperature differences for the two skin-web combinations for either wing appear to be approximately the same. However, the temperature differences for the original wing are somewhat higher than for the duplicate; this might be attributed to the higher heating rate incurred by the original wing and possibly to poorer thermal conductance of the joints in this model. Whatever the reason, the greater actual temperature differences

undoubtedly produced greater induced thermal stresses in model MW-1. That this was so is partly substantiated by the earlier failure of this wing.

When the results of figure 9(a) for skin and web 3 are replotted as dimensionless temperatures, as in figure 9(b), the experimental data for the two wings, using indicated values of T_{aw}, appear to be in much better agreement. This would imply that the thermal conductance was not significantly different in the joints in the skin-web combinations of the two models, and, therefore, that the higher actual temperature differences experienced by model MW-1 were mainly due to the higher rate of aerodynamic heating. Comparison of the test data with calculated values obtained by using the method given in reference 4 and Van Driest's aerodynamic heat-transfer coefficients shows results similar to those previously obtained for the skin temperatures in that the test data are somewhat higher than the predicted values. Since the Van Driest method underestimates the skin temperatures by approximately this amount, little of the difference between the calculated values and the test data is due to any joint resistance to internal heat flow.

Temperatures in the solid leading-edge section.- Figure 10(a) shows the measured temperatures in the solid leading-edge section plotted against time. Since test conditions ended shortly after 11 seconds, data beyond this time are questionable; however, the temperature of thermocouple 1 (the highest model temperature measured) appears to be approaching a limit toward the end of test conditions (11.3 seconds). At this time thermocouple 1 had reached a temperature of 402° F, a value which is only slightly lower than the average indicated value of T_{aw} of 418° F. Thermocouples 2, 3, and 4 have progressively lower temperatures, as expected, since these thermocouples are progressively farther from the leading edge and the heated surface.

Figure 10(b) shows a plot of the dimensionless temperatures along the center line of the solid leading-edge section and along the skin in the adjacent bay for a time of 8 seconds. The temperature distribution, predicted from average Van Driest's heat-transfer coefficients, generally underestimates the test data and shows only fair agreement except for the three lowest data points, which could however be somewhat low as a result of impedance to the conductive flow of heat caused by the joint between the overlapping skin and the solid leading-edge piece. The method for calculating the temperature distributions is the same as that described in reference 2.

Experimental Pressures

The experimental model pressures and pressure differences are listed in Table III. These experimental pressures can be expected to reflect not only any change in the stagnation pressure but also any local or overall angular movement, either static or dynamic, experienced by the model during a test. After the stagnation pressure subsided from its peak value at about 2 seconds, the pressure differences and the pressures in the center bay and $1\frac{7}{8}$ inches from the trailing edge were the only ones which remained essentially constant. The remaining pressures were fairly steady until shortly after 6 seconds, then the pressures between the leading edge and center bay decreased slightly with time, whereas along the latter half of the chord, except for the trailing edge, the pressures increased appreciably with time. The decrease in stagnation pressure just after 6 seconds may account for most of the general decrease in pressure over the forward portion of the model but obviously does not explain the continued increase over the rearward half. The fact that many of the pressures continue to change with time may be partly the result of some increasing distortion of the chordwise cross section occurring as the result of a corresponding growth in the induced thermal stresses. Some additional change in pressure levels, particularly in the rear, can probably be attributed to the flutter; the pressure gages are insensitive to the model vibrations but tend to register the approximate average pressure experienced during such vibrations. During the second flutter period the amplitudes grew in intensity, and the effect on the pressure gages was to increase their readings as the vibrations became more violent.

Although the pressure differences from one surface to the other remained constant, they indicate that the pressures $1\frac{7}{8}$ inches from both the leading and trailing edges were approximately 1 psi less on the surface containing the pressure orifices than on the opposite surface. This condition tends to indicate that the side of the model with the pressure orifices was at some small negative angle of attack; the calculated angle of attack corresponding to the experimental pressure difference was approximately 0.8° at the leading edge and approximately 1.3° at the trailing edge.

The experimental data in the form of chordwise pressure-coefficient distributions at both 5 and 10 seconds are shown in figure 11 along with a calculated distribution obtained by using second-order small-perturbation theory. The agreement between the theory and experimental data is fairly good but is better near the forward portion of the model. Poorer agreement should be expected toward the rear because of the minor effects of disturbances coming from the exit (along the vertical sides) of the nozzle,

reflections of the leading-edge disturbances from the jet boundaries, and some three-dimensional effects created by the pressure difference between the moving jet stream and the surrounding still air. At 10 seconds the agreement between theory and experiment over the rearward half of the model is better than the agreement at 5 seconds because of the increase in pressure coefficients during the latter portion of the test. However, this increase is probably the result of various factors such as chordwise distortion and flutter, and the better agreement is therefore somewhat meaningless.

Strain Results

Ten of the wire strain gages used in the test were attached in the chordwise direction to the underside of the skin (fig. 4) primarily to obtain information about the frequency and phasing of vibration or flutter of the individual skin panels; the resulting information was considered to be reliable and was used in conjunction with the motion pictures to determine the frequencies and confirm the type of flutter experienced by the model. In addition, experimental spanwise strains were obtained at the center line of the third inboard stiffener (gage 5) and in the skin in the center bay and last bay (gages 6 and 11), corrected for lack of complete temperature compensation, and compared with calculated strains. Actually, the strain gages pick up strains due to pressure loading in addition to strains resulting from the self-equilibrating thermal stresses, but in the present case the strains due to external (pressure) loading were considered small enough to be neglected. Thus, the discussion deals only with strains associated with thermal stresses and does not include any strains due to simple thermal expansion. Correction of the experimental strains for temperature effects is accompanied by some uncertainty. Calibration data were obtained only to the maximum curing temperature of 285° F, which is appreciably lower than the recommended curing temperature of 350° F, and under steady-state conditions, which were considerably different from the transient test conditions. The computed spanwise strains were calculated from known chordwise temperature distributions according to the method of reference 8. Since complete experimental chordwise temperature distributions were not available, calculated chordwise temperature distributions were used. The available experimental temperatures agreed with the assumed chordwise temperatures almost as well as the corresponding agreement for model MW-1 shown in reference 1. For the strain calculations, the wing cross section was idealized into 40 elements.

Gage 5 on the stiffener remained relatively cool and thus required little temperature correction. The strain obtained from this gage is plotted in figure 12 and can be seen to be in excellent agreement with the calculated strain. However, this agreement is undoubtedly somewhat

fortuitous since the agreement between the assumed temperature distribution and the experimental temperatures was not this excellent. The strains from gages 6 and 11 attached to the skin required appreciable temperature corrections. The resulting strains for the two gages were generally nearly twice the calculated strains (fig. 12). This discrepancy is due in part to differences in the assumed and actual temperature distributions, to inaccuracies in the method of correcting the strains for temperature effects, and, in very small measure, to the effect of differential pressure loading on the skin.

The magnitudes of the thermal stresses corresponding to the strains shown in figure 12 may be of interest. The trend of the histories of the stresses is similar to that of the strains except that the differences between the experimental and calculated skin stresses are somewhat greater than for the strains. At 8 seconds the experimentally obtained stresses were approximately 16.6, -7.0, and -4.2 ksi compared with calculated values of 16.3, -3.1, and -1.6 ksi at the locations of gages 5, 6, and 11, respectively. The experimental stress at the location of gage 5 on the stiffener can be obtained directly from the strain for gage 5 since the state of stress is essentially uniaxial at that point. However, since a biaxial state of stress exists in the skin, the strains from chordwise gages 7 and 12, considered as being at the same locations as gages 6 and 11, respectively, were used in obtaining the spanwise stresses at these two points. These chordwise effects largely account for the fact that the differences between the experimental and calculated skin stresses are greater than for the strains.

Accelerometer

Whereas the wire strain gages reflected only the actual straining of the individual panels, the accelerometer (also attached to the skin) depicted any chordwise motion to which the wing was subjected. The oscillograph trace showed a dominant frequency response which matched that of the wire strain gages and which increased in amplitude during the starting disturbance and the periods of flutter, as also verified by the wire strain gages and the motion pictures.

Model Failure

As described earlier, model MW-1-(2) experienced two periods of flag-waving or chordwise bending type of flutter, a mild or nondestructive form of very small amplitudes from about 5.81 to 6.29 seconds with frequencies between 215 and 205 cycles per second, and a more severe form which began at 8.14 seconds and became catastrophic as the test progressed, with the first visible signs of failure occurring at 11.16 seconds.

During this second flutter period the frequency dropped from about 185 to 115 cycles per second. The lowering of the flutter frequency from the first to the second flutter period, accompanied by increasing amplitudes, clearly demonstrates a loss in structural stiffness resulting from the aerodynamic heating. The behavior of the wing during the second flutter period and during the initial stages of destruction is shown in figure 13 and 14, respectively. The remainder of the model after the test is shown in figure 15.

In contrast, the original wing (model MW-1, ref. 1) experienced only one flutter period which began at 7.5 seconds and resulted in visible signs of failure at 8.8 seconds and total destruction by 9.9 seconds. The low-speed motion pictures (24 frames per second) of this model provide the only tangible evidence of the behavior of the model and indicate that failure was apparently preceded by skin buckling (chordwise buckling of the individual skin panels between webs) and some sort of flutter. On the other hand, in the test of model MW-1-(2) the high-speed motion pictures (up to 1,600 frames per second) revealed that this model did not experience any skin buckling but underwent a definite chordwise or flag-waving type of flutter prior to failure. However, it is believed that the actions of the two wings preceding failure, although somewhat different in detail, were essentially similar in principle in that flutter involving chordwise distortions led to destruction. Prior to the onset of buckling or flutter, the models remained steady - a fact which indicated that they were capable of withstanding the aerodynamic forces, without aerodynamic heating, at least at zero angle of attack. Thus, the aerodynamic heating must have provided the means necessary to make the models fail.

Aerodynamic heating induces both longitudinal and chordwise stresses in these structures; both types of stresses lower the structural stiffness. Additional losses in stiffness - usually small - will also occur as the result of the effect of increase in temperature on the elastic moduli. As stated in reference 1, the restraints of the unheated, heavy tip and root bulkheads could have caused chordwise compressive skin stresses of approximately the same magnitude as the critical stress; apparently, in model MW-1 these thermal stresses reached the critical stress and caused the skin panels to buckle. Such buckling constitutes a loss in stiffness and lowers the resistance of the structure to flutter. However, the slower heating of model MW-1-(2) should have delayed the buildup of these chordwise stresses; thus, this model apparently reached the critical condition wherein the model began to flutter before chordwise skin buckling occurred.

Spanwise thermal stresses are introduced by the restraint of the cool webs and cool portions of the solid leading- and trailing-edge members to the expansion of the hot skin and hot portions of the leading

and trailing edges. The spanwise thermal stresses also change the stiffness of the model, particularly by reducing the stiffness of the hotter portions of the skin where large spanwise compressive stresses result, thereby reducing the resistance of the structure to flutter. Because of the slower heating of model MW-1-(2) these spanwise thermal stresses developed more slowly for model MW-1-(2) than for the original model and, consequently, the destruction of this model began later. (A slightly lower dynamic pressure would also have contributed to a later failure of model MW-1-(2).) Reference 9 shows that such stresses reduce the natural frequencies for the mode shapes of similar cantilevered structures, particularly where chordwise bending is concerned.

When flutter occurs unaccompanied by aerodynamic heating, the model will flutter at a given frequency in a mode which is some combination of its natural modes; when aerodynamic heating is present the frequency will be reduced and the flutter mode shape may be modified. How severely the aerodynamic heating affects the flutter modes and frequencies of the MW-1 type of wing is presently unknown. For the two models under discussion, it would seem that (1) the thermal stresses and changes in moduli resulting from the aerodynamic heating changed the effective stiffness substantially from a safe to an unsafe region so that the models fluttered and failed, or (2) the models were originally only marginally safe at zero angle of attack and Mach number 2 sea-level conditions without aerodynamic heating, in which case only a slight decrease in stiffness would have been necessary to produce flutter. Without recourse to an actual flutter analysis, or additional tests, one cannot tell which condition prevailed. In the design of supersonic airfoils, a knowledge of the flutter characteristics and the effects of aerodynamic heating in changing the behavior of the structure may well be crucial to the design.

Since flutter is produced by a combination of aerodynamic forces and structural response, the aerodynamic forces are significant. These aerodynamic forces are related to the stagnation pressure; any change in the stagnation pressure reflects a similar change in both the static and dynamic pressures. During the test of model MW-1-(2) the stagnation pressure varied slightly; a temporary maximum value of over 119 psia occurred at about 2 seconds (fig. 5(a)), but the model did not flutter, apparently because the model had not yet been weakened by aerodynamic heating. As the test progressed, fairly appreciable thermal stresses developed which seemingly lowered the structural stiffness to the threshold of flutter whence, accompanied by a slight increase in stagnation pressure, the model fluttered with very small amplitudes from 5.81 to 6.29 seconds. Then, approximately coincident with about a 3- to 4-percent drop in stagnation pressure, the model ceased fluttering until the transient aerodynamic heating reduced the structural stiffness and more than

counterbalanced the small loss in energy of the aerodynamic forces, with the result that the model then fluttered catastrophically.

The absence of any internal chordwise ribs signifies that these multiweb wings have little structural restraint against chordwise distortion; in addition, the connections of the web flanges to the skin probably approach the condition of pin-end supports in that they offer little restraint against rotation and thereby allow the skin to buckle over several bays. Thus, this type of wing may easily be deformed in the shape of a chordwise wave wherein the deflection near the front is opposite the deflection in the rearward portion, with the deflections at the rear more pronounced. Both models failed essentially in this manner, model MW-1 with a more or less localized flutter near the rear and model MW-1-(2) with a rippling or flag-waving flutter across the chord but with the biggest deflections also near the rear.

CONCLUDING REMARKS

A 2024-T3 aluminum-alloy multiweb wing, model MW-1-(2), of 40-inch chord and semispan was tested at a Mach number of 2 under simulated sea-level conditions, and temperatures, pressures, and strains were measured with the following results:

The temperature data showed, as expected, that the highest recorded temperature was obtained near the leading edge, that the skin temperatures decreased across the chord, and that the interior temperatures were lower than surface temperatures. "Indicated" values of the aerodynamic heat-transfer coefficient obtained from the skin temperature data showed a large amount of scatter, and the agreement with values obtained by using Van Driest's method was only fair. The experimental temperatures were generally higher than temperatures calculated by using Van Driest's heat-transfer coefficients.

The experimentally obtained pressure coefficients across the chord changed slightly during the test but were generally in fair agreement with values calculated according to second-order small-perturbation theory.

Most of the recorded strains were used to aid in confirming the shape of the flutter experienced by the model and in establishing the flutter frequencies. Spanwise compressive skin strains obtained at two locations were about twice the calculated strain values. The tensile strain obtained for only one spanwise stiffener showed very good agreement with the calculated strain.

The model experienced a dynamic failure late in the test as a result of excessive chordwise flutter brought on by a reduction in structural stiffness resulting from thermal stresses and some reduction in the elastic moduli.

Langley Aeronautical Laboratory,
National Advisory Committee for Aeronautics,
Langley Field, Va., March 14, 1958.

REFERENCES

1. Heldenfels, Richard R., Rosecrans, Richard, and Griffith, George E.: Test of an Aerodynamically Heated Multiweb Wing Structure (MW-1) in a Free Jet at Mach Number 2. NACA RM L53E27, 1953.

2. Griffith, George E., Miltonberger, Georgene H., and Rosecrans, Richard: Tests of Aerodynamically Heated Multiweb Wing Structures in a Free Jet at Mach Number 2 - Two Aluminum-Alloy Models of 20-Inch Chord With 0.064- and 0.081-Inch-Thick Skin. NACA RM L55F13, 1955.

3. Rosecrans, Richard, Vosteen, Louis F., and Batdorf, William J., Jr.: Tests of Aerodynamically Heated Multiweb Wing Structures in a Free Jet at Mach Number 2 - Three Aluminum-Alloy Models and One Steel Model of 20-Inch Chord and Span With Various Internal Structures and Skin Thicknesses. NACA RM L57H01, 1957.

4. Miltonberger, Georgene H., Griffith, George E., and Davidson, John R.: Tests of Aerodynamically Heated Multiweb Wing Structures in a Free Jet at Mach Number 2 - Two Aluminum-Alloy Models of 20-Inch Chord With 0.064-Inch-Thick Skin at Angles of Attack of 0° and $\pm 2^{\circ}$. NACA RM L57H19, 1957.

5. Smith, W. A., and Kops, E. A.: Heat Insulation Effectivity of Selected Paint Finishes Investigation of Model General. Rep. No. 8675 (Contract No. AF33(600)-5942), Convair, Sept. 22, 1954.

6. Chauvin, Leo T., and deMoraes, Carlos A.: Correlation of Supersonic Convective Heat-Transfer Coefficients From Measurements of the Skin Temperature of a Parabolic Body of Revolution (NACA RM-10). NACA TN 3623, 1956. (Supersedes NACA RM L51A18.)

7. Van Driest, E. R.: Turbulent Boundary Layer in Compressible Fluids. Jour. Aero. Sci., vol. 18, no. 3, Mar. 1951, pp. 145-160, 216.

8. Heldenfels, Richard R.: The Effect of Nonuniform Temperature Distributions on the Stresses and Distortions of Stiffened-Shell Structures. NACA TN 2240, 1950.

9. Vosteen, Louis F., McWithey, Robert R., and Thomson, Robert G.: Effect of Transient Heating on Vibration Frequencies of Some Simple Wing Structures. NACA TN 4054, 1957.

TABLE I

AERODYNAMIC TEST DATA

Nominal angle of attack, deg	0
Mach number	2.00
Tunnel stagnation pressure, psia	113
[a]Tunnel stagnation temperature, ^{o}F	574
Free-stream static pressure, psia	14.5
Free-stream dynamic pressure, psi	40.6
Free-stream temperature, ^{o}F	114
Free-stream velocity, fps	23.5×10^{2}
Free-stream density, slugs/cu ft	21.2×10^{-4}
Speed of sound, fps	11.7×10^{2}
Reynolds number per foot, 1/ft	12.3×10^{6}

[a]As noted in the section entitled "Test Conditions," this value may be in error because of uncertainty concerning the true cold-junction temperature.

TABLE II

TEMPERATURES FOR MODEL MW-1-(2)

t, sec	Temperature, °F, at thermocouple -																									
	1	2	3	4	5	6	7	9	10	11	12	13	14	15	16	17	18	19	20	21	22	26	28	30	31	33	34
0	88	88	87	87	83	85	82	82	81	79	80	81	79	79	78	79	79	84	82	77	77	76	74	78	74	76	71
1	115	101	88	88	107	108	106	101	102	83	81	97	97	81	79	78	97	101	101	96	95	92	90	92	89	85	71
2	165	126	95	95	143	145	144	132	133	94	81	129	131	92	81	79	134	133	137	133	133	124	118	117	114	105	74
3	215	156	107	108	182	186	184	169	164	113	82	163	157	108	87	79	160	162	165	160	159	149	141	144	137	130	80
4	258	186	124	123	209	218	216	199	190	131	87	190	179	124	91	83	183	189	191	184	183	173	163	168	158	151	88
5	292	212	142	140	233	247	245	228	214	150	95	218	200	139	100	87	204	212	214	206	205	195	184	190	178	170	98
6	320	238	160	158	252	271	268	253	236	169	111	241	219	153	113	100	228	234	237	228	228		203	209	197	188	106
7	343	260	177	174	270	293	289	276	255	186	119	254	237	169	120	101	213		254	243	242		223	226	214	202	116
8	361	280	196	190	286	311	307	296	273	201	133	272	258	181	132	111			271	261	262		240	242	229	216	127
9	377	299	213	206	300	326	322	321	294	222	152	297	267	198									258	257	244	230	
10	389	314	229	222	313		336			238	168		285	212									273	270		240	
11	400	329	245	237			347			255	182			228									281				
12	406	340	261	251			356																				
13	409	348	276	261																							
14	407	353	287	270																							
15	402	354	294	277																							

TABLE III

PRESSURES FOR MODEL MW-1-(2)

t, sec	Pressure, psia, at orifice -										[a]Pressure difference, psia, between orifice -	
	2	4	5	6	7	8	9	10	11	13	1 and 3	12 and 14
0	14.63	14.63	14.63	14.63	14.63	14.63	14.63	14.63	14.63	14.63	0	0
1	19.13	16.06	13.96	13.03	15.03	15.38	14.85	14.13	13.93	14.52	2.42	-.11
2	19.03	17.63	16.72	15.23	15.28	13.03	11.38	10.63	10.43	9.53	.37	-.77
3	20.18	18.93	17.88	15.48	13.13	11.15	10.53	10.28	10.23	9.78	-.73	-.82
4	20.00	18.58	17.53	15.18	12.93	11.48	11.33	10.68	10.58	9.93	-.85	-.86
5	20.01	18.63	17.58	15.20	12.96	11.48	11.23	10.58	10.53	9.92	-.88	-.87
6	20.03	18.78	17.73	15.38	13.13	11.38	10.98	10.38	10.33	9.78	-.90	-.88
7	19.98	18.48	17.48	15.03	12.92	11.73	11.53	10.78	10.68	9.93	-.91	-.87
8	19.58	18.33	17.38	15.01	12.92	11.91	11.63	10.88	10.73	9.95	-.93	-.87
9	19.35	18.13	17.30	14.90	12.78	12.21	11.88	11.06	11.03	9.93	-1.04	-.93
10	19.26	18.08	17.25	14.83	12.80	12.38	11.98	11.10	11.10	9.92	-1.07	-.94
11	18.23	17.18	16.57	14.03	15.68	15.13	12.78	11.63	11.58	9.23	-1.15	-.86
12	15.53	14.98	14.49	14.28	12.28	17.13	14.48	13.88	11.66	11.78	-1.25	.68
13	14.13	17.93	19.43	13.63	11.58	17.06	14.28	13.73	11.81	13.60	.52	.40
14	14.82	14.46	14.28	14.13	12.48	17.13	14.38	13.80	12.00	14.41	.35	.15
15	14.63	14.63	14.63	14.63	13.48	17.03	14.69	14.00	12.33	14.58	0	0

[a]Negative sign indicates pressure is higher on side opposite pressure orifices.

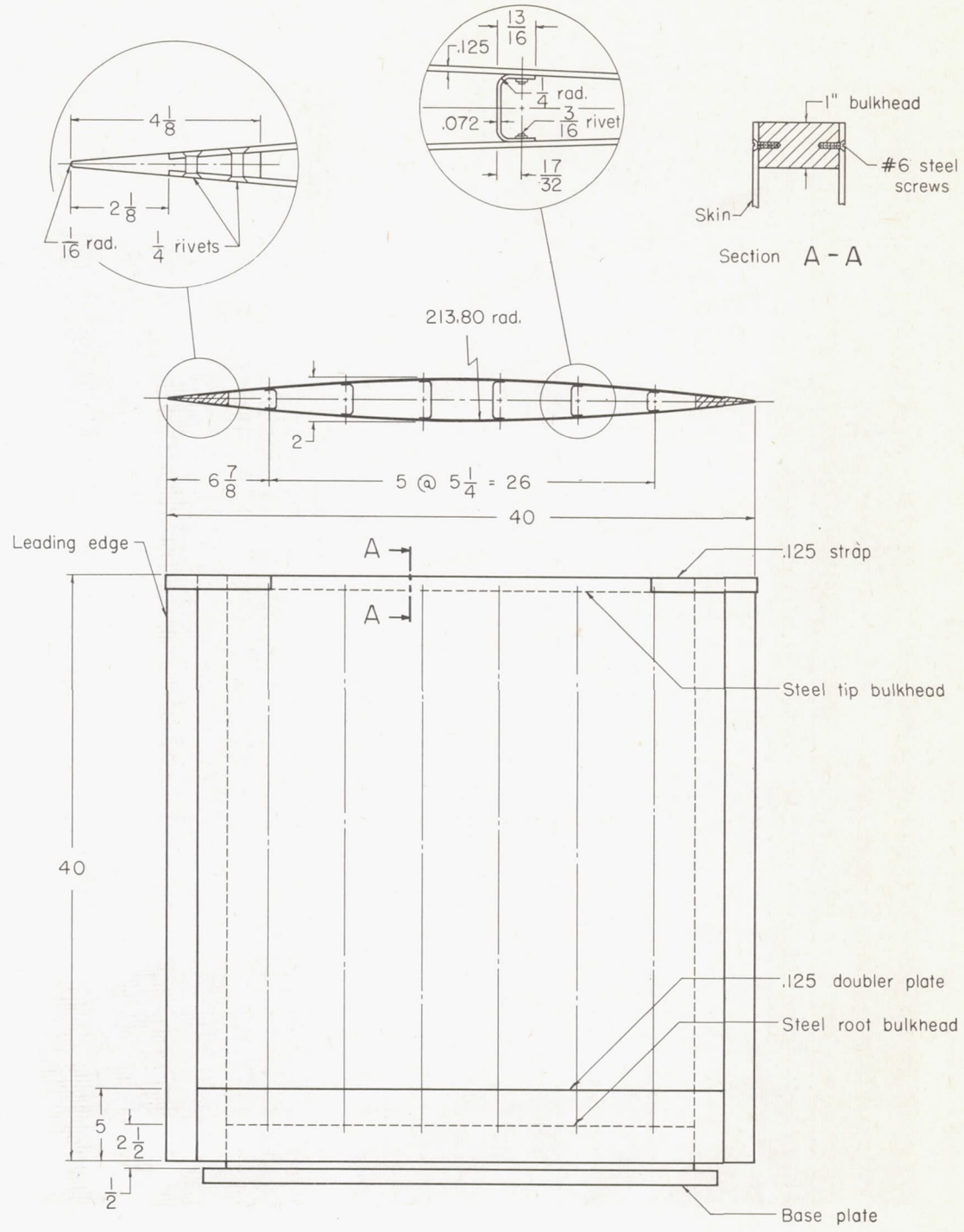


Figure 1.- Dimensions of multiweb wing model MW-1-(2). Material 2024-T3 unless otherwise specified. All dimensions are in inches.

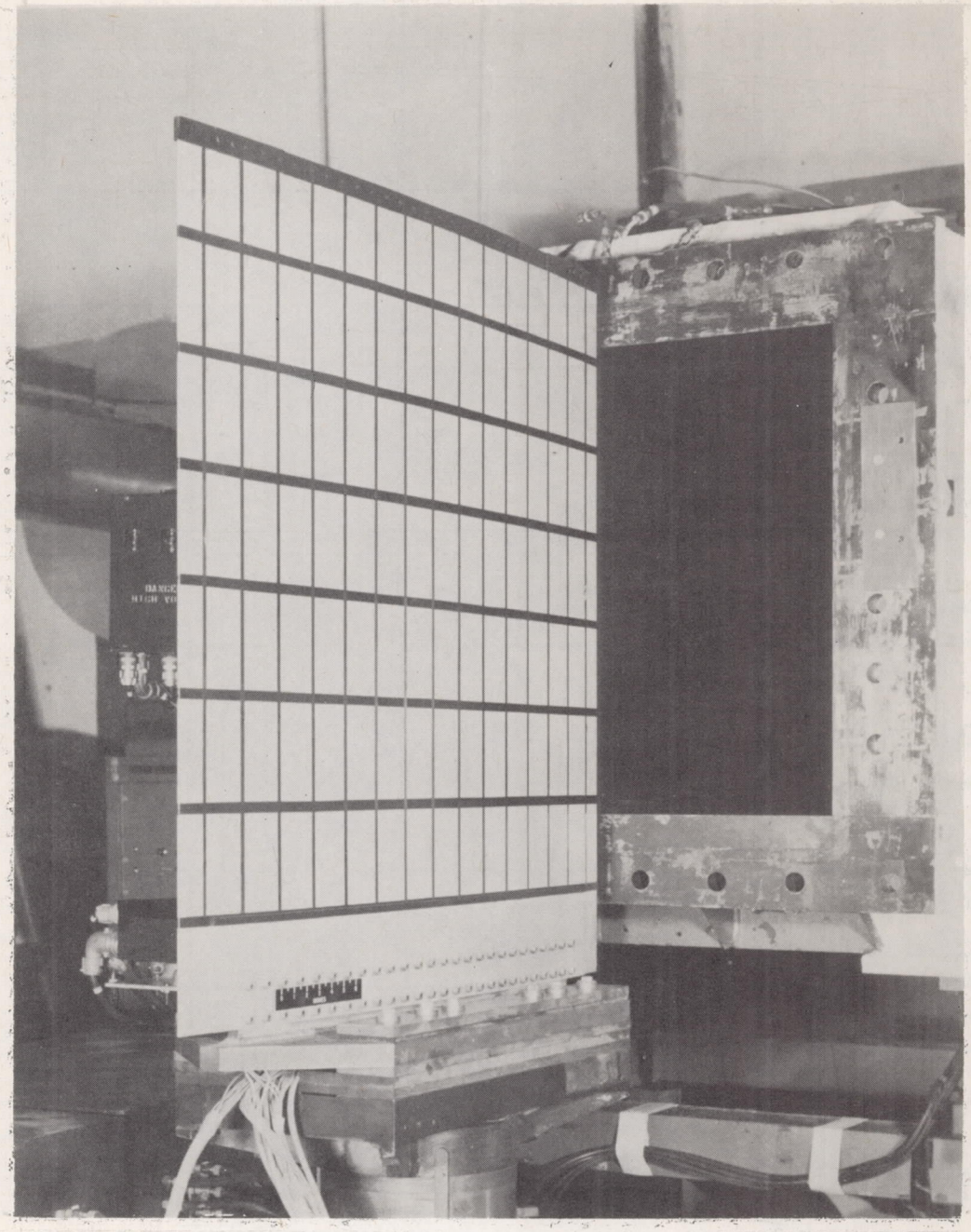


Figure 2.- Model in place at nozzle exit prior to test. L-84729

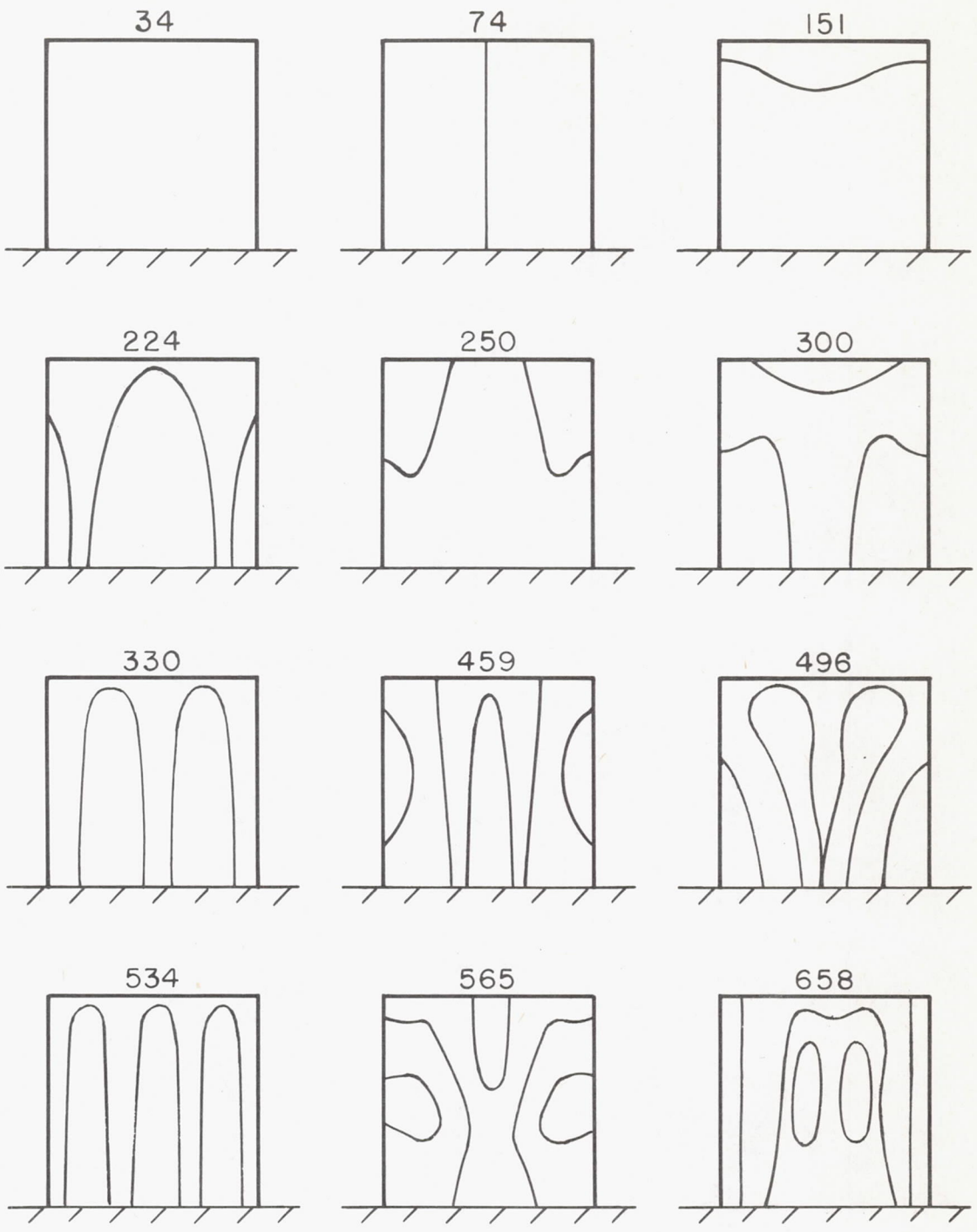


Figure 3.- Natural modes and frequencies. (Solid lines indicate node lines; the numbers refer to the corresponding natural frequencies in cycles per second.)

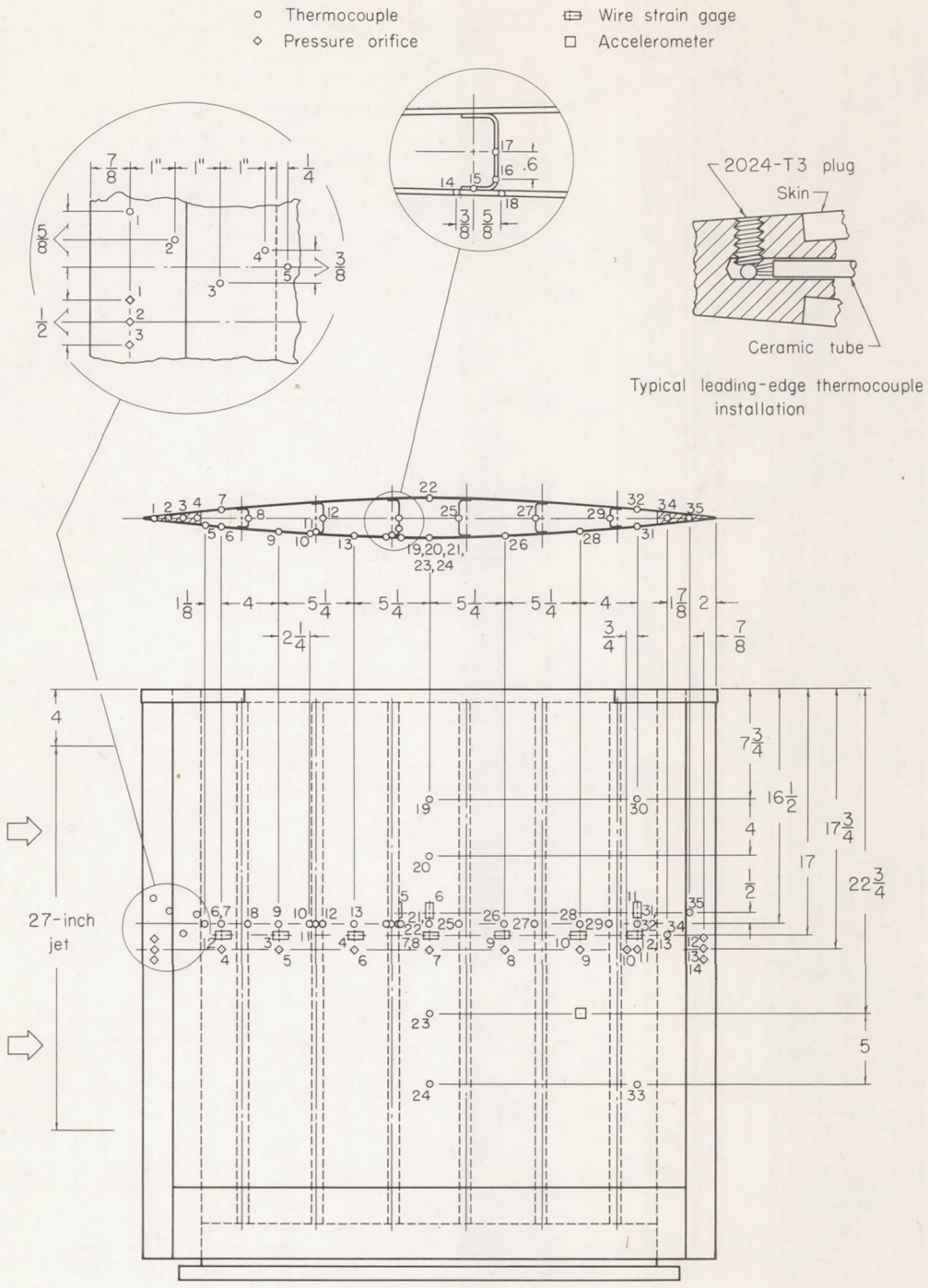
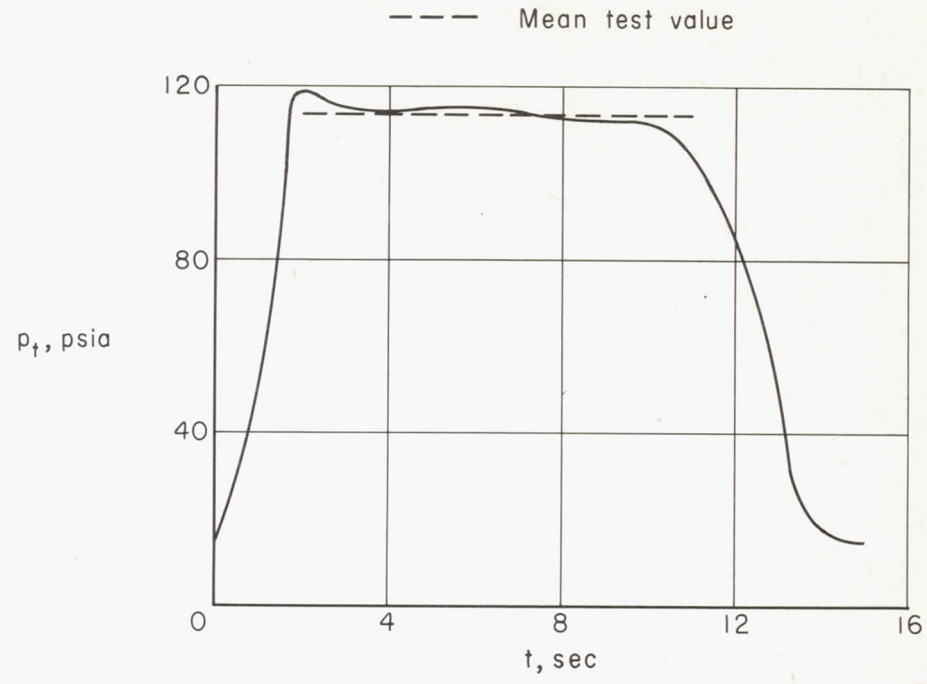
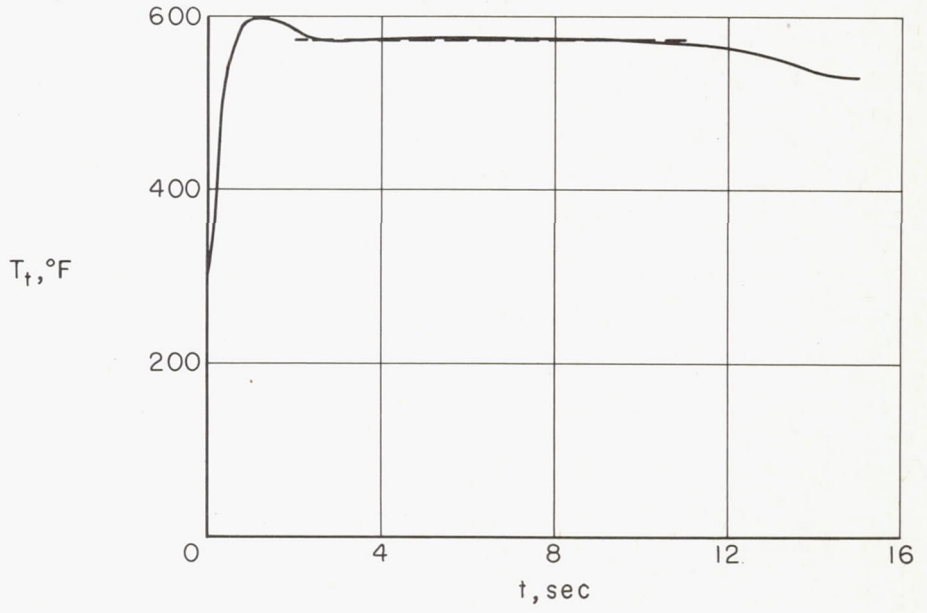


Figure 4.- Model instrumentation. Wire strain gages 1 and 13 and pressure orifices 3 and 14 are on far skin. (All dimensions are in inches.)



(a) Stagnation pressure.



(b) Stagnation temperature.

Figure 5.- Stagnation pressure and temperature.

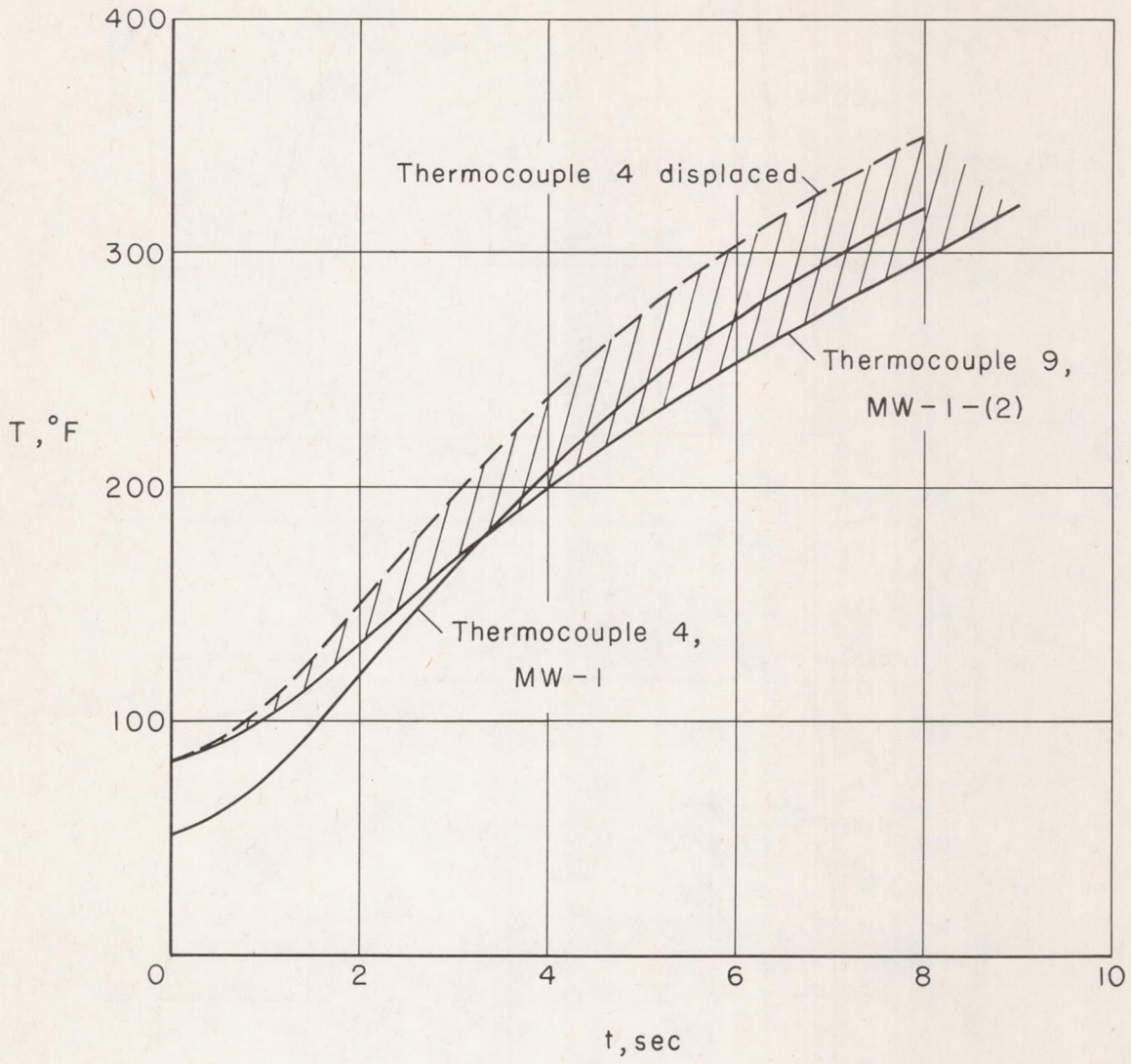


Figure 6.- Typical skin temperature histories.

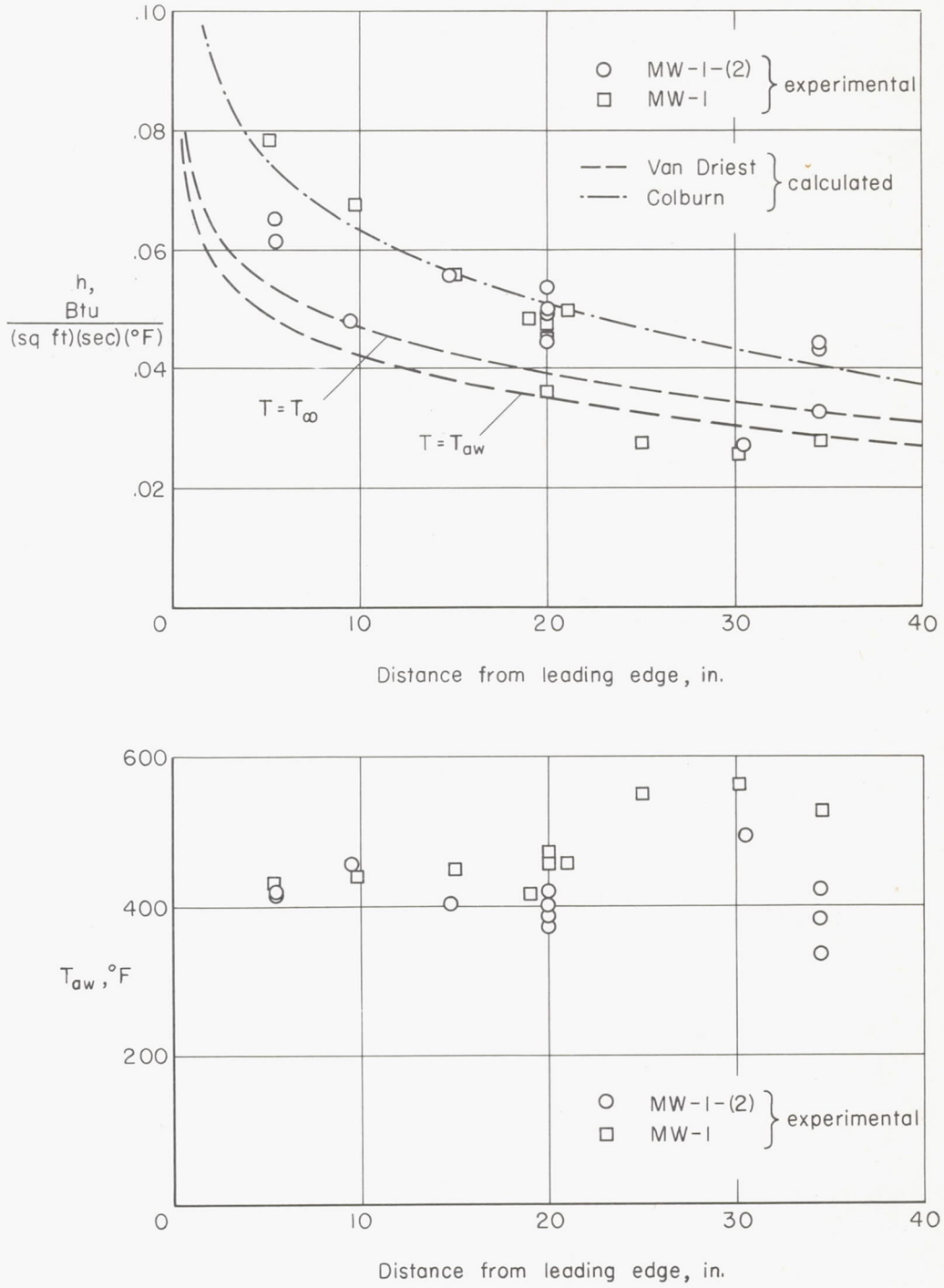


Figure 7.- Chordwise variation of aerodynamic heat-transfer coefficient and adiabatic wall temperature.

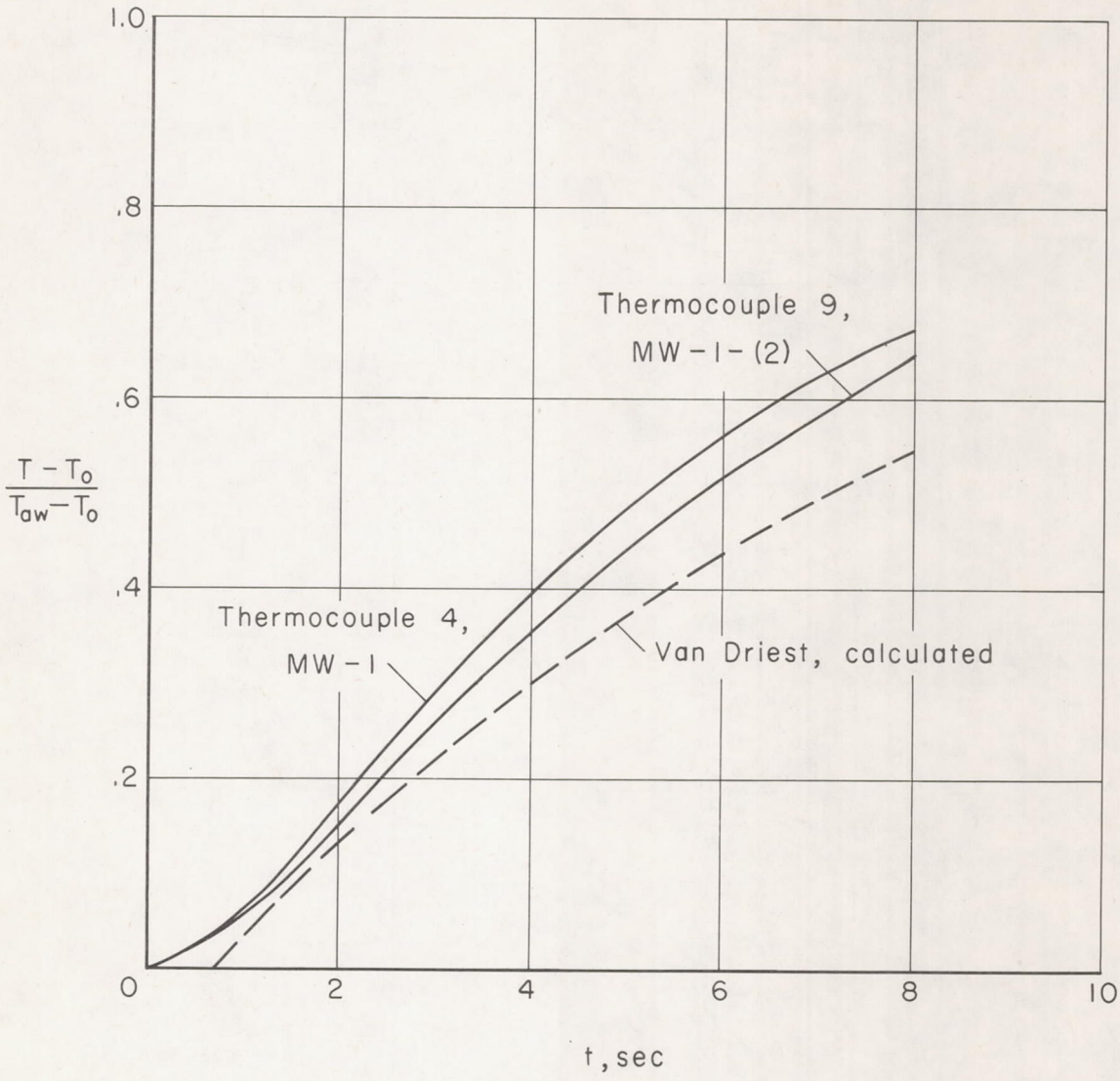
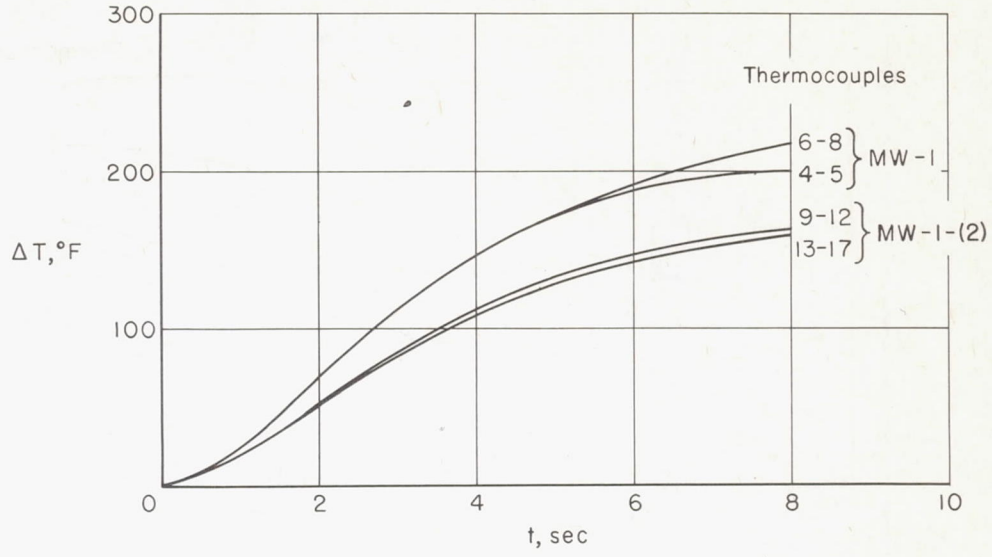
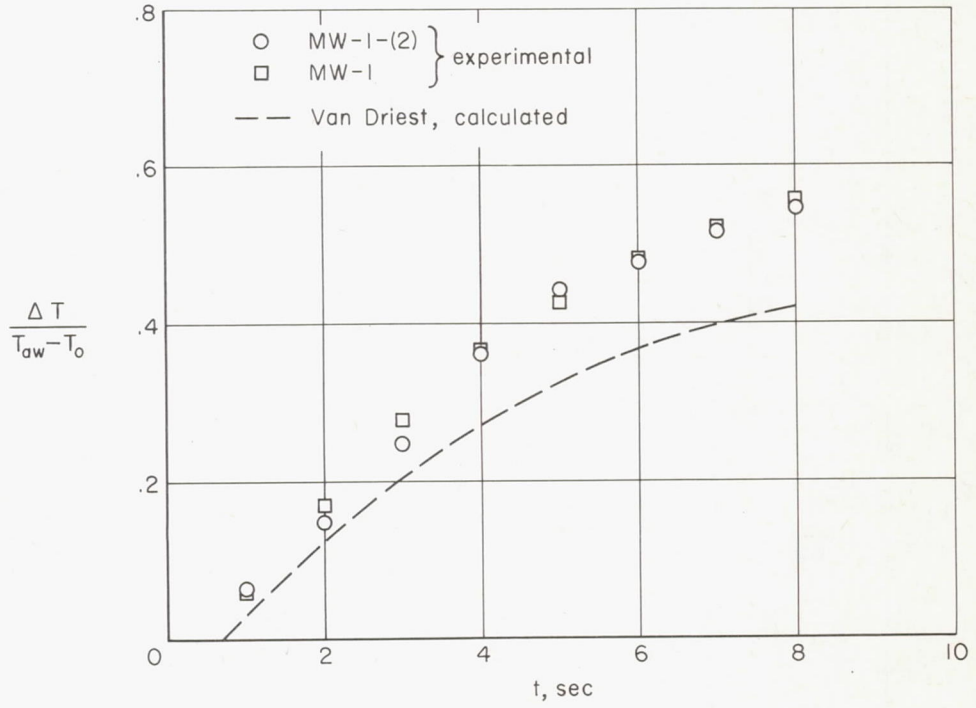


Figure 8.- Typical skin temperature histories in dimensionless form.

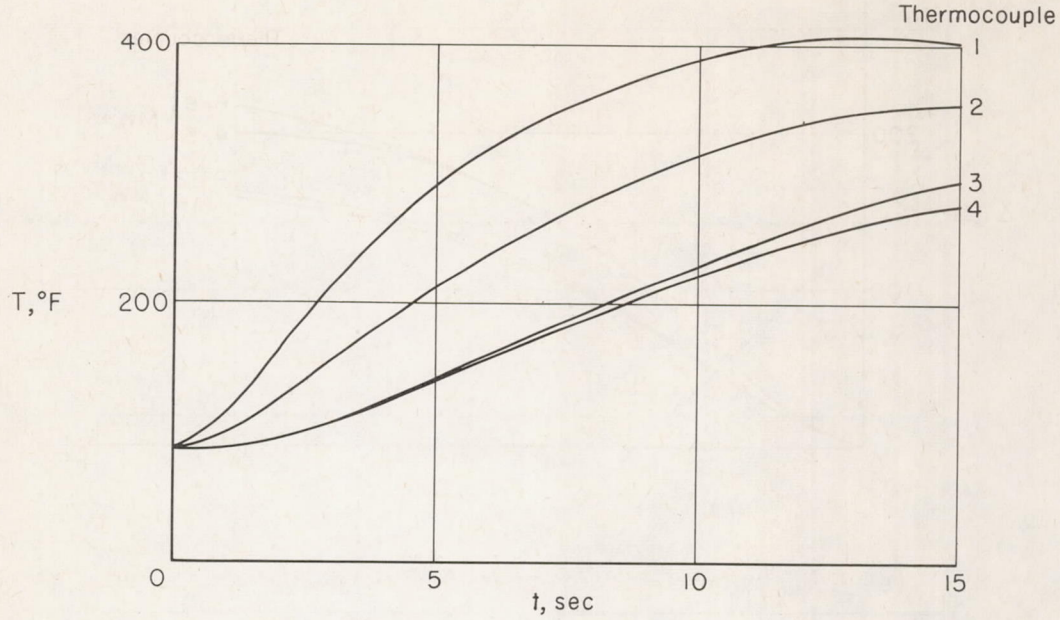


(a) Temperature differences for skin and webs 2 and 3.

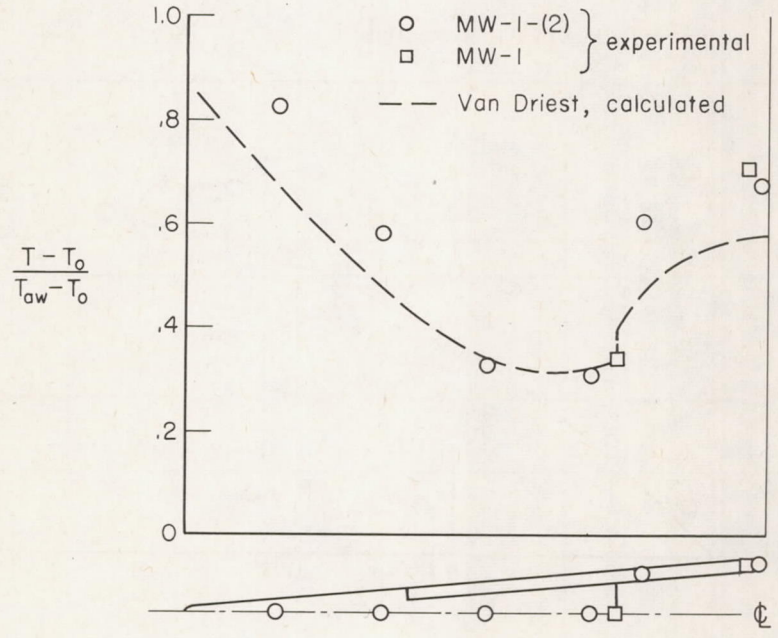


(b) Nondimensional temperature differences for skin and web 3.

Figure 9.- Skin and web temperature differences.



(a) Leading-edge temperatures, model MW-1-(2) only.



(b) Leading-edge temperature distribution at 8 seconds.

Figure 10.- Temperatures in solid leading-edge section.

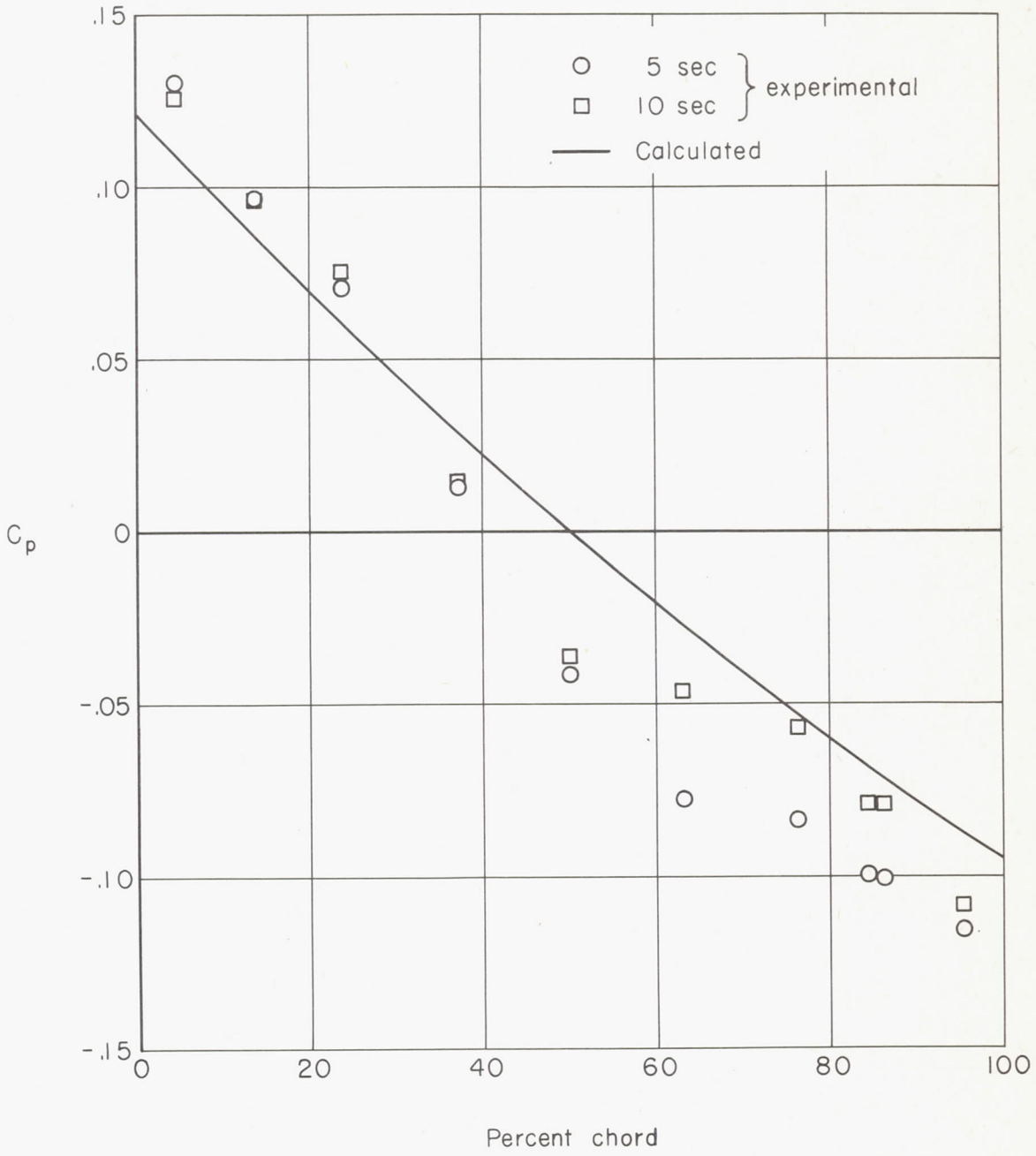


Figure 11.- Chordwise pressure distributions.

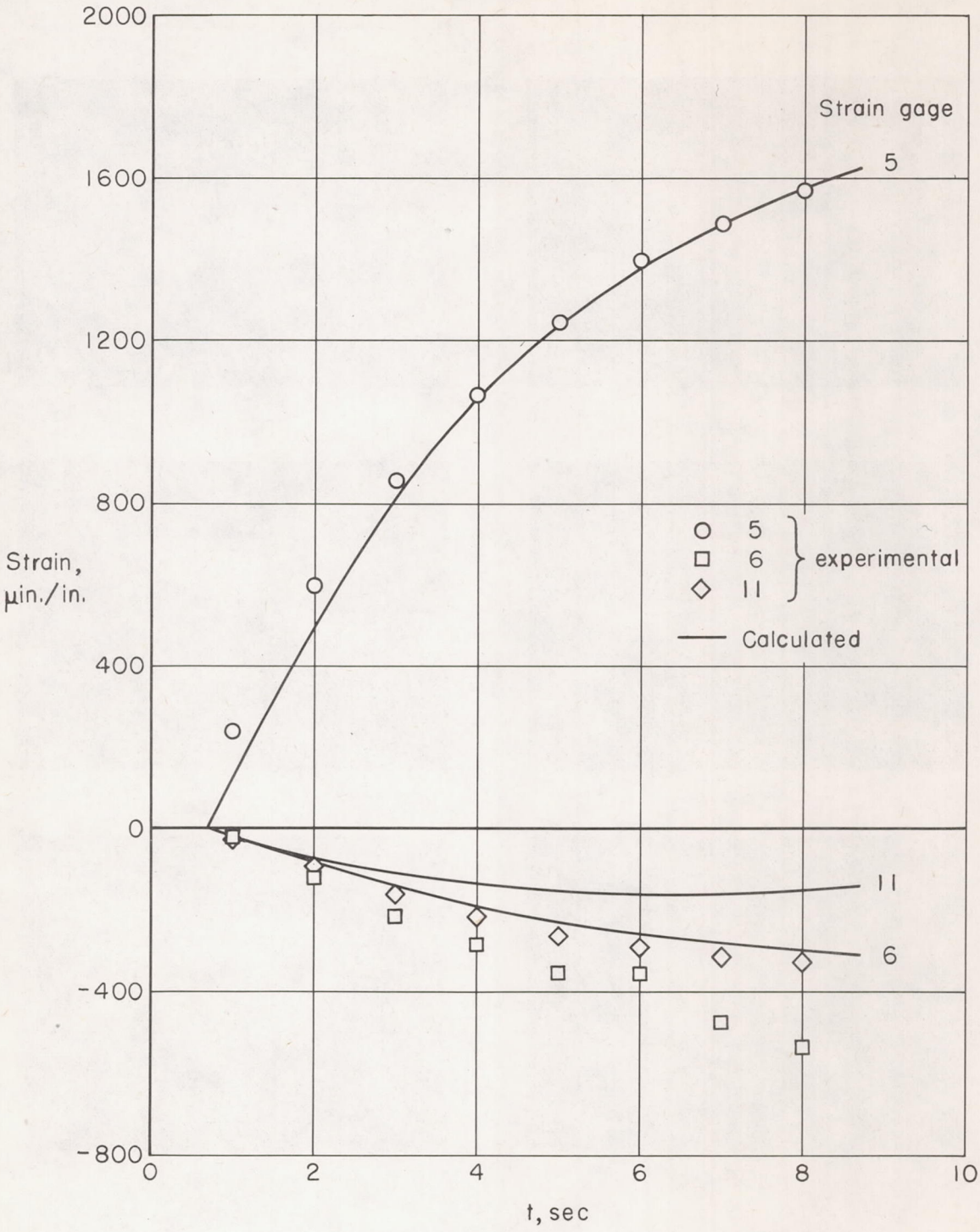
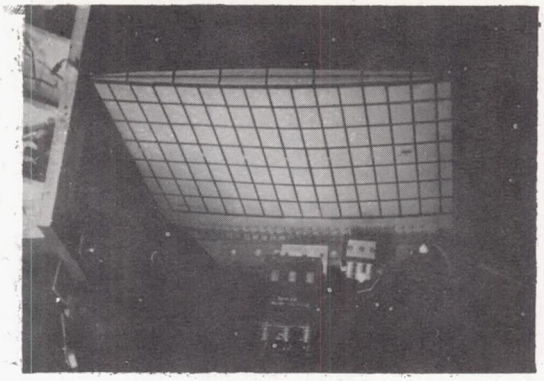
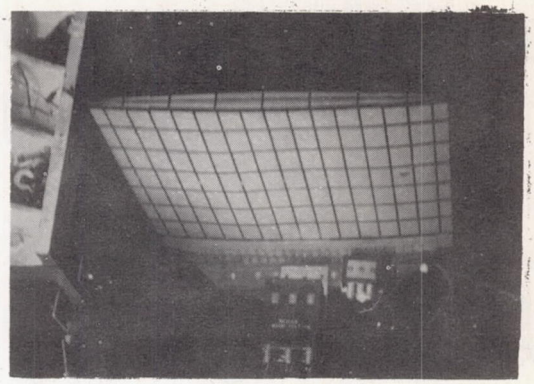


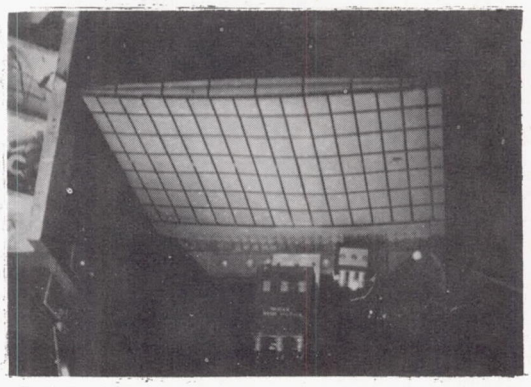
Figure 12.- Spanwise strains.



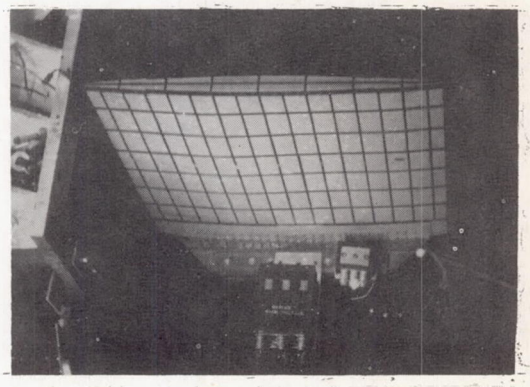
t = 10.88 sec



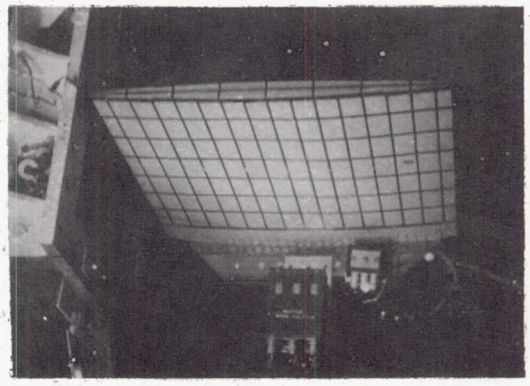
t = 10.90 sec



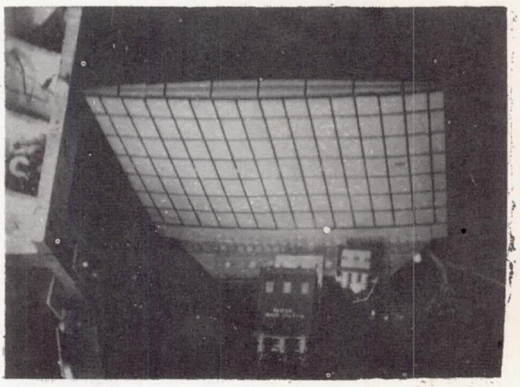
t = 10.92 sec



t = 10.94 sec

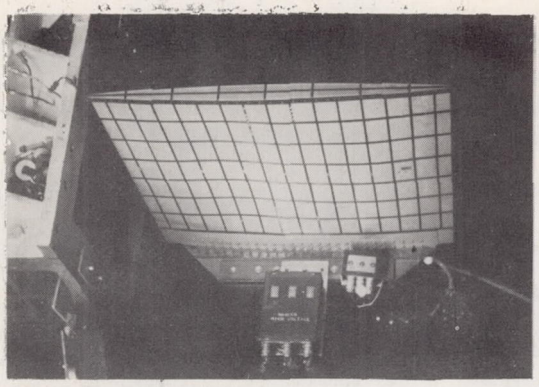


t = 10.96 sec

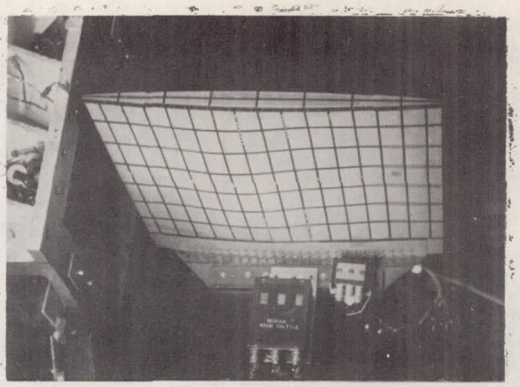


t = 11.04 sec

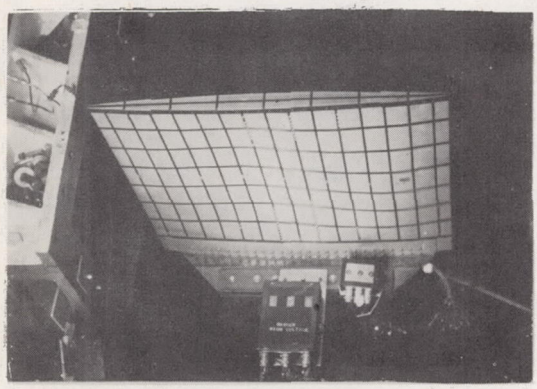
Figure 13.- Model flutter leading to failure. L-58-178



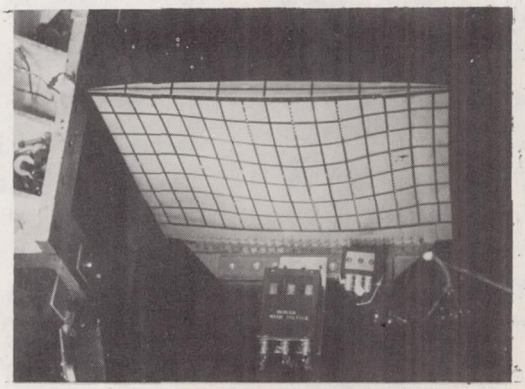
t = 11.16 sec



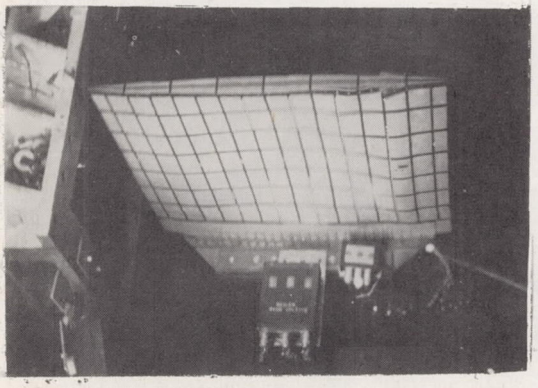
t = 11.18 sec



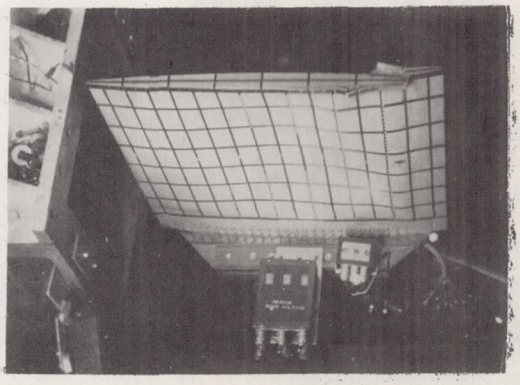
t = 11.20 sec



t = 11.24 sec



t = 11.30 sec



t = 11.40 sec

L-58-179

Figure 14.- Model flutter during the initial stages of destruction.

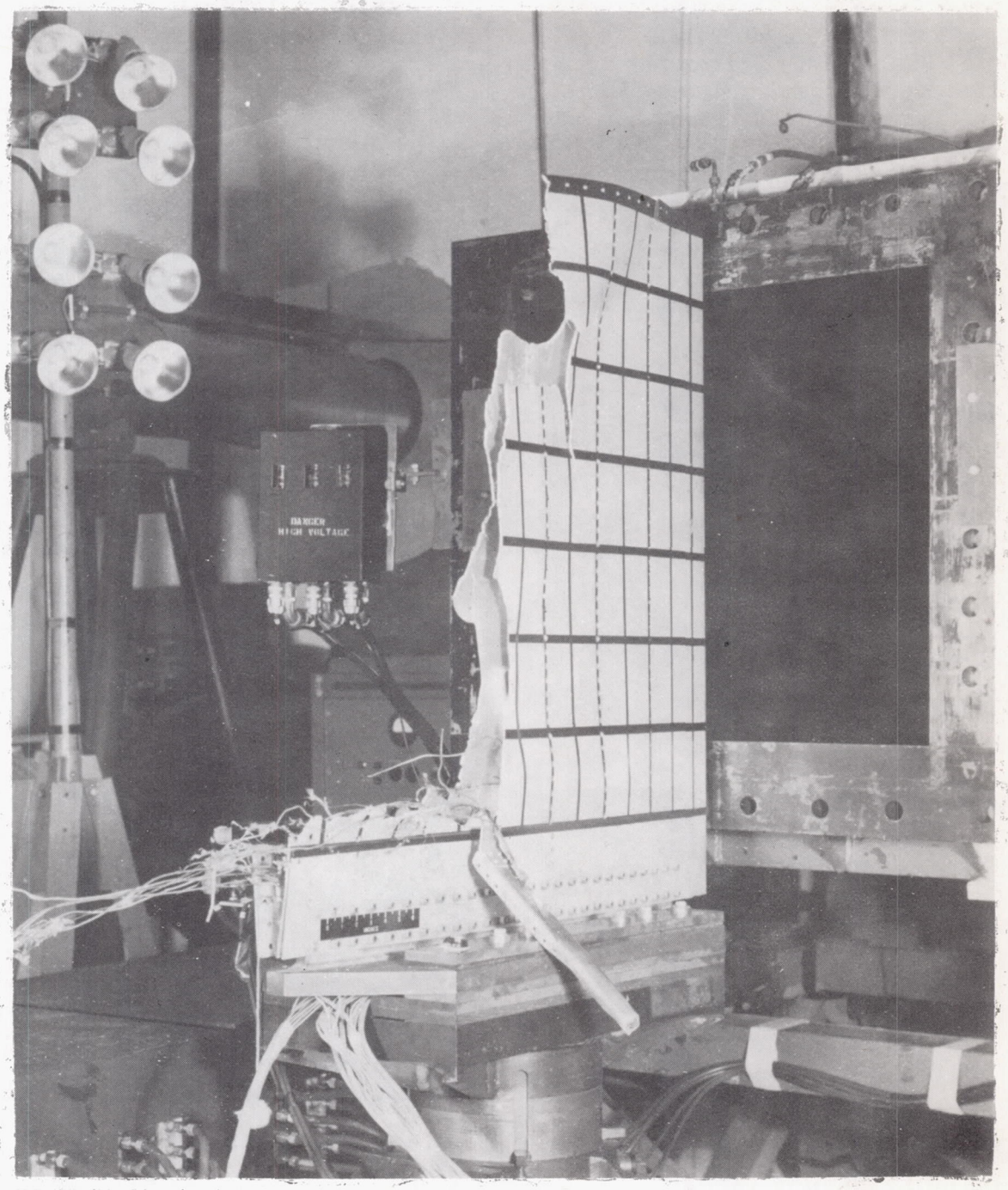


Figure 15.- Remainder of model after test. L-84731